ISSN 0001-4338, Izvestiya, Atmospheric and Oceanic Physics, 2017, Vol. 53, No. 2, pp. 142–155. © Pleiades Publishing, Ltd., 2017.
Original Russian Text © E.M. Volodin, E.V. Mortikov, S.V. Kostrykin, V.Ya. Galin, V.N. Lykosov, A.S. Gritsun, N.A. Diansky, A.V. Gusev, N.G. Yakovlev, 2017, published in Izvestiya Rossiiskoi Akademii Nauk, Fizika Atmosfery i Okeana, 2017, Vol. 53, No. 2, pp. 164–178.

Simulation of Modern Climate with the New Version of the INM RAS Climate Model

E. M. Volodin[a, b, c, *], E. V. Mortikov[a, b], S. V. Kostrykin[a], V. Ya. Galin[a], V. N. Lykosov[a, b], A. S. Gritsun[a, c], N. A. Diansky[a], A.V. Gusev[a], and N. G. Yakovlev[a]

[a] *Institute of Numerical Mathematics, Russian Academy of Sciences, Moscow, 119333 Russia*
[b] *Moscow State University, Moscow, 119991 Russia*
[c] *Institute of Applied Physics, Russian Academy of Sciences, Nizhny Novgorod, 603950 Russia*
**e-mail: volodinev@gmail.com*

Received December 25, 2015; in final form, January 25, 2016

Abstract—The INMCM5.0 numerical model of the Earth's climate system is presented, which is an evolution from the previous version, INMCM4.0. A higher vertical resolution for the stratosphere is applied in the atmospheric block. Also, we raised the upper boundary of the calculating area, added the aerosol block, modified parameterization of clouds and condensation, and increased the horizontal resolution in the ocean block. The program implementation of the model was also updated. We consider the simulation of the current climate using the new version of the model. Attention is focused on reducing systematic errors as compared to the previous version, reproducing phenomena that could not be simulated correctly in the previous version, and modeling the problems that remain unresolved.

Keywords: model, climate, atmosphere, ocean, parameterization

DOI: 10.1134/S0001433817020128

1. INTRODUCTION

Climate models are currently one of the main instruments of climate research, understanding its past changes, and predicting future ones. There is a hierarchy of climate models: the simplest, globally averaged [1]; models of intermediate complexity [2]: and, finally, coupled models of general circulation of the atmosphere and ocean. The INMCM5.0 model, like its previous versions [3], belongs to the latter class of climate models. Apart from two main blocks—the general circulation of the atmosphere and ocean—modern climate models include other components of the climate system. This can be, for example, models of the land surface, its active layer and vegetation, sea ice, atmospheric chemistry, the carbon cycle, and some others. The development of climate models is on the path of increasing the number of these blocks, so that we can talk about evolution of climate models in a model of the Earth system. The international scientific community is performing the Coupled Model Intercomparison Project (CMIP). The essence of this project is that all climate models undergo the same basic set of experiments, and then the authors of these models can participate in various subprojects, i.e., conduct additional experiments. The latest such comparison, the CMIP5 (Phase 5), took place in 2010–2013. A description of experiments within this project is given in [4]; the results of some of these experiments with the INMCM4 model can be found in [5]. The results of this comparison are described also in Chapters 9 and 12 of the first volume of 5th Assessment Report of the Intergovernmental Panel on Climate Change (IPCC) [6]. The next phase of the project (CMIP6) should take place in 2016–2018. One of the main goals of creating a new version of the INMCM climate model (INMCM5.0) is to participate in this program.

2. DESCRIPTION OF THE MODEL AND NUMERICAL EXPERIMENT

The INMCM5.0 climate model consists of two main blocks: the General Circulation of the Atmosphere and the Ocean General Circulation. Hydrodynamics equations in the atmospheric block are solved in the quasi-static approximation with the finite difference method. The longitude, latitude, and σ coordinate are used as coordinates. Differential equations and the finite-difference scheme are presented in [7, 8]. The finite-difference scheme is of second order in space and first order in time (the semi-implicit scheme is used, in which gravity waves are considered implicitly). Formally, there are no exact conservation laws in the finite-difference model. Resolution for longitude and latitude is $2° \times 1.5°$, and there are 73 vertical levels. Compared to the INMCM4 version of the model, the vertical resolution in the stratosphere is higher in the new model and is about 500 m. The upper boundary of the calculating area lies at the altitude of about 60 km. This is significantly higher than in the previous version, where it was at the altitude of about 30 km, which is required for the proper simulation of dynamics of the stratospheric. The time step in the Dynamic block is 4 min. The procedures of physical parameterization are called once per hour, and procedures for calculating radiation are called once in every 3 h.

Like in the previous version, the INMCM5.0 model uses the parameterization of atmospheric radiation [9]; deep and shallow convection [10]; orographic [11] and nonorographic [12] gravity-wave drag; and processes in the soil, land surface, and vegetation [7]. Compared to the previous version, the scheme for the calculation of clouds and condensation is amended. In the original version of the model, the cloud amount was calculated diagnostically, independently of the calculation of condensation, and depended on the relative humidity [7]. The water content (ice content) of clouds was also calculated diagnostically and depended only on temperature. In the new version of the model, the proportion of the cells occupied by clouds and cloud water content is calculated prognostically, according to [13].

The model of the atmospheric dynamics is complemented by the aerosol block, in which predictive equations are calculated for the concentration of ten substances: coarse and fine fractions of dust and sea salt, sulfur dioxide, sulfate aerosol, and hydrophilic and hydrophobic forms of black and organic carbon. In the radiation block, both the direct and indirect effects of aerosols are taken into account. A detailed description of the aerosol block and its application in climate models is described in [14].

In the ocean block, which represents a model of general circulation of the ocean, finite difference equations are solved on a grid with a resolution of $0.5° \times 0.25°$ in longitude and latitude and 40 sigma levels vertically. Compared to the previous version, resolution in each of the horizontal coordinates was increased by a factor of two. To avoid problems related to the simulation of dynamics near the poles, we use a grid in generalized spherical coordinates, where the South Pole is at the same place as the geographical pole, and the North Pole is placed on the territory of Siberia, outside the computational domain. The time step in the ocean dynamics block is 15 min. The hydrodynamics equations of the ocean and methods of their solution are presented in [15, 16]. In this version of the model, unlike the previous one, the explicit scheme is used for solving the transport equation (rather than implicit one, based on the coordinate splitting method), and an iterative method (instead of a direct one) is used for solving equations for the sea level and barotropic components of velocity. This was done to adapt the algorithm of the model to massively parallel computers; the parallel implementation of the code for ocean dynamics simulation is described in [17]. Apart from the two main blocks, the model of climate system includes a sea-ice evolution block [18].

Software implementation of the climate-system model allows one to distribute calculations associated with the dynamics of the atmosphere, ocean dynamics, and evolution of trace gases in the atmosphere into different groups of parallel processes using the MPI library. The atmospheric and ocean blocks share the results of their calculations every 2 h of simulated time. The atmospheric dynamics data enter the aerosol block at each dynamic step, and the information about the aerosol concentrations is passed to the block of the atmosphere dynamics once every 2 h. Data exchanges with the aerosol block are performed asynchronously with additional buffering messages. For the current version of the atmospheric model, which includes the transport of ten substances, the selection of an equal number of cores for the atmospheric dynamics and aerosol block is sufficient to reduce the computation time by up to a factor of two. Software implementation of the INMCM5.0 model and its scalability on modern computer systems are discussed in more detail in [19]. The proposed calculation of species transport using independent groups of computational processes seems to us more versatile and efficient than the introduction of complementary and only partially active parallel processes proposed in [20] for models of the atmosphere, including an aerosol block.

The optimal numbers of processor cores for a given spatial resolution, as derived for the Lomonosov supercomputer in Moscow State University and supercomputer of the Joint Supercomputer Center of Russian Academy of Science, are 96 for atmospheric and aerosol blocks and 192 for the ocean block, i.e., 384 cores in total for the whole model. Under these conditions, the count rate is about 6 years of modeled time for one day of computer time.

A numerical experiment was carried out with the model to reproduce the current climate, for which the concentration of trace gases, sources of anthropogenic aerosols, solar radiation flux, and distribution of vegetation were set to be relevant to the mid-twentieth century. The duration of the simulated period was 80 years. Initial data for the calculation was obtained as a result of previous calculations. They correspond to the model climate, so there is no significant trend in the atmosphere and upper ocean layer during the period of time considered in the experiment. A small trend in the deep ocean, as well as in other climatic models, takes place. These simulations are compared with available observations. For a comparison of temperature, wind speed, and pressure, the data of the ERA [21] and NCEP [22] reanalysis are used; for precipitation, the data [23] are taken as observations. The ocean temperature and salinity data are compared with the data [24].

3. RESULTS OF NUMERICAL SIMULATION

3.1. Atmosphere and Surface

Globally mean values of the heat balance components and other parameters characterizing the "atmo-

Integrated parameters of the observed and model climate.

Title	Observations	INMCM3	INMCM4	INMCM5
Incoming solar radiation at TOA	341.3 [26]	341.7	341.8	341.4
Outgoing solar radiation at TOA	96–100 [26]	97.5 ± 0.1	96.2 ± 0.1	98.5 ± 0.2
Outgoing longwave radiation at TOA	236–242 [26]	240.8 ± 0.1	244.6 ± 0.1	241.6 ± 0.2
Solar radiation absorbed by surface	154–166 [26]	166.7 ± 0.2	166.7 ± 0.2	169.0 ± 0.3
Solar radiation reflected by surface	22–26 [26]	29.4 ± 0.1	30.6 ± 0.1	30.8 ± 0.1
Longwave radiation balance at surface	–54 to 58 [26]	–52.1 ± 0.1	–49.5 ± 0.1	–63.0 ± 0.2
Solar radiation reflected by atmosphere	74–78 [26]	68.1 ± 0.1	66.7 ± 0.1	67.8 ± 0.1
Solar radiation absorbed by atmosphere	74–91 [26]	77.4 ± 0.1	78.9 ± 0.1	81.9 ± 0.1
Direct hear flux from surface	15–25 [26]	27.6 ± 0.2	28.2 ± 0.2	18.8 ± 0.1
Latent heat flux from surface	70–85 [26]	86.3 ± 0.3	90.5 ± 0.3	86.1 ± 0.3
Cloud amount, %	64–75 [27]	64.2 ± 0.1	63.3 ± 0.1	69 ± 0.2
Solar radiation-cloud forcing at TOA	–47 [26]	–42.3 ± 0.1	–40.3 ± 0.1	–40.4 ± 0.1
Longwave radiation-cloud forcing at TOA	26 [26]	22.3 ± 0.1	21.2 ± 0.1	24.6 ± 0.1
Near-surface air temperature, °C	14.0 ± 0.2 [26]	13.0 ± 0.1	13.7 ± 0.1	13.8 ± 0.1
Precipitation, mm/day	2.5–2.8 [23]	2.97 ± 0.01	3.13 ± 0.01	2.97 ± 0.01
River water inflow to the World Ocean, 10^3 km^3/year	29–40 [28]	21.6 ± 0.1	31.8 ± 0.1	40.0 ± 0.3
Snow coverage in Feb., mil. km^2	46 ± 2 [29]	37.6 ± 1.8	39.9 ± 1.5	39.4 ± 1.5
Permafrost area, mil. km^2	10.7–22.8 [30]	8.2 ± 0.6	16.1 ± 0.4	5.0 ± 0.5
Land area prone to seasonal freezing in Northern Hemisphere, mil. km^2	54.4 ± 0.7 [31]	46.1 ± 1.1	48.3 ± 1.1	51.6 ± 1.0
Sea ice area in Northern Hemisphere in March, mil. km^2	13.9 ± 0.4 [32]	12.9 ± 0.3	14.4 ± 0.3	14.5 ± 0.3
Sea ice area in Northern Hemisphere in Sept., mil. km^2	5.3 ± 0.6 [32]	4.5 ± 0.5	4.5 ± 0.5	6.1 ± 0.5

Heat flux units are given in W/m^2; the other units are given with the title of corresponding parameter. Where possible, ± shows standard deviation for annual mean value.

sphere–ocean–cryosphere" system are shown in table. The components of the radiation balance in the model generally fit into the range of estimates from observational data. An exception is solar radiation absorbed and reflected by the surface, which is somewhat exaggerated in all versions of the model, apparently due to the underestimated value of the solar radiation reflected by the atmosphere. The longwave radiation balance of the surface in the latest version of the model is also somewhat low.

In the current version of the model, the sensible heat flux has decreased in comparison with the previous versions and become close to observational data. The same happened to the latent heat flux. This occurred presumably as a result of both the new parameterization of condensation and clouds and accounting for involvement of the atmospheric boundary layer at the top edge, which resulted in a change in its stratification and hence in a change of fluxes from the surface; the formulae for the calculation of fluxes from the surface does not change. Modification of the calculation scheme for clouds led to a better agreement of longwave radiation-cloud forcing with assessment made on the basis of satellite measurements, which is mainly due to the increase in the optical thickness of the upper clouds in the tropics. At the same time, the radiation-cloud forcing in the solar part of spectrum was underestimated.

The heat balance at the top of the atmosphere is 1.3 W/m^2; the heat balance on the surface is 1.1 W/m^2. The difference of 0.2 W/m^2 is due to the absorption of solar and heat radiation in a fictitious layer located above the first level of the model. The total heat flux on the surface is partially spent on melting of the ice in Greenland and Antarctica, the mass balance of which is not calculated in the model, and in part leads to a slow trend in the deeper layers of the ocean. However, the time variation in the heat content of the deep ocean layers, which is close to the mentioned above heat difference, is common to all modern climate models.

Integral parameters of the cryosphere generally correspond to the observed range of these variables, except for the area of permafrost, which is significantly understated in the latest version of the model. This occurs because the thermal conductivity coefficient of the upper layers of soil (which contains moss and fallen leaves) in the model, although having smaller values than in the depth, is apparently still too high when compared to its real value.

Integrated climate indicators in the latest version of the model remained approximately at the same level of

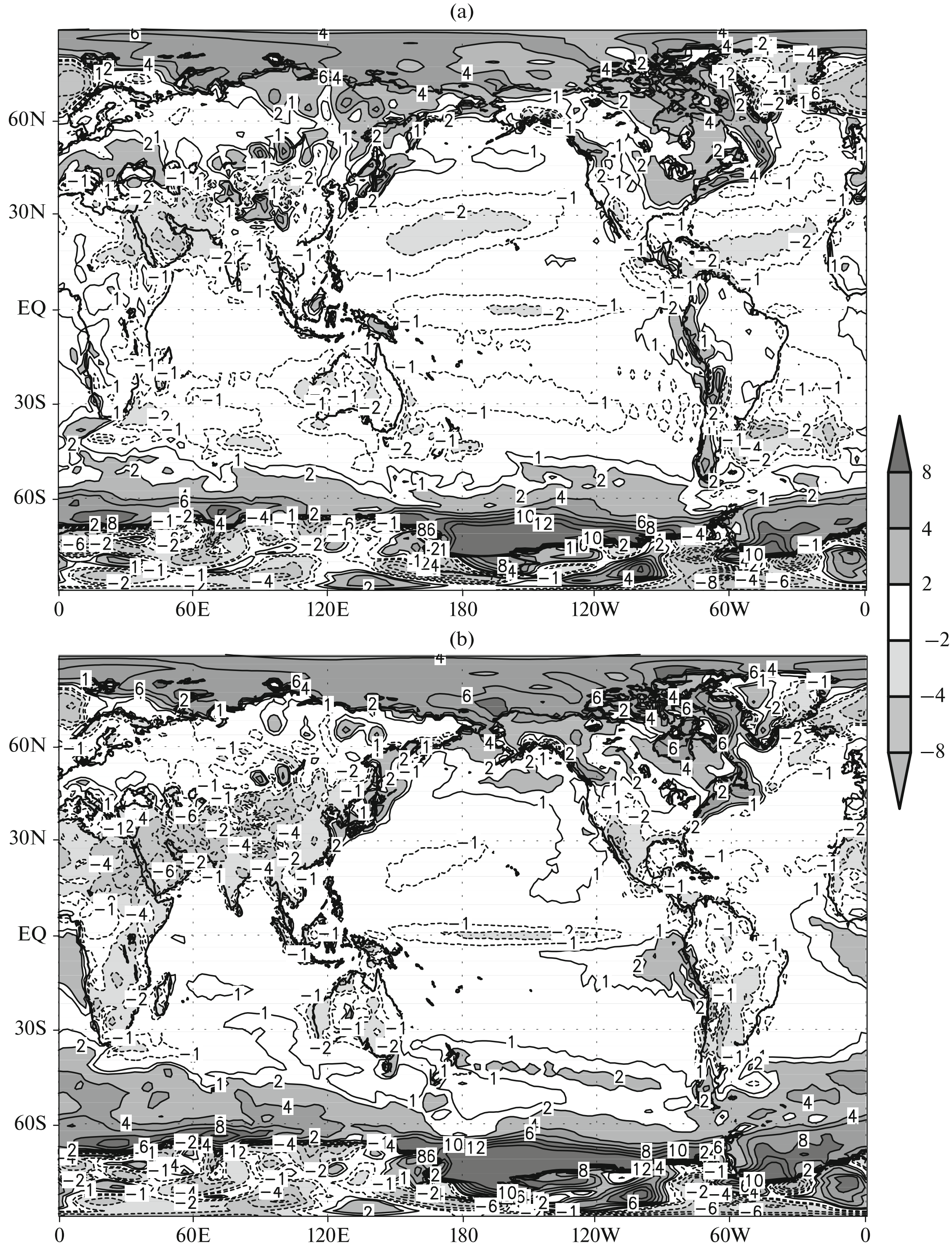

Fig. 1. Difference in the annual mean surface temperature (K) between the model and the ERA reanalysis: (a) in the INMCM5.0 model; (b) in the INMCM4.0 model.

compliance with the observed data as in the previous version, or were slightly improved.

Figure 1 shows an annual mean error in the near-surface air temperature (NSAT) in the INMCM4.0 and INMCM5.0 versions of the model. The NSAT error in the INMCM5.0 version remains roughly the same as it was in the INMCM4.0. It is this spatial distribution in the error of the ocean surface temperature (including its underestimation in the center of the Pacific Ocean near the equator and overestimation along the Pacific coast

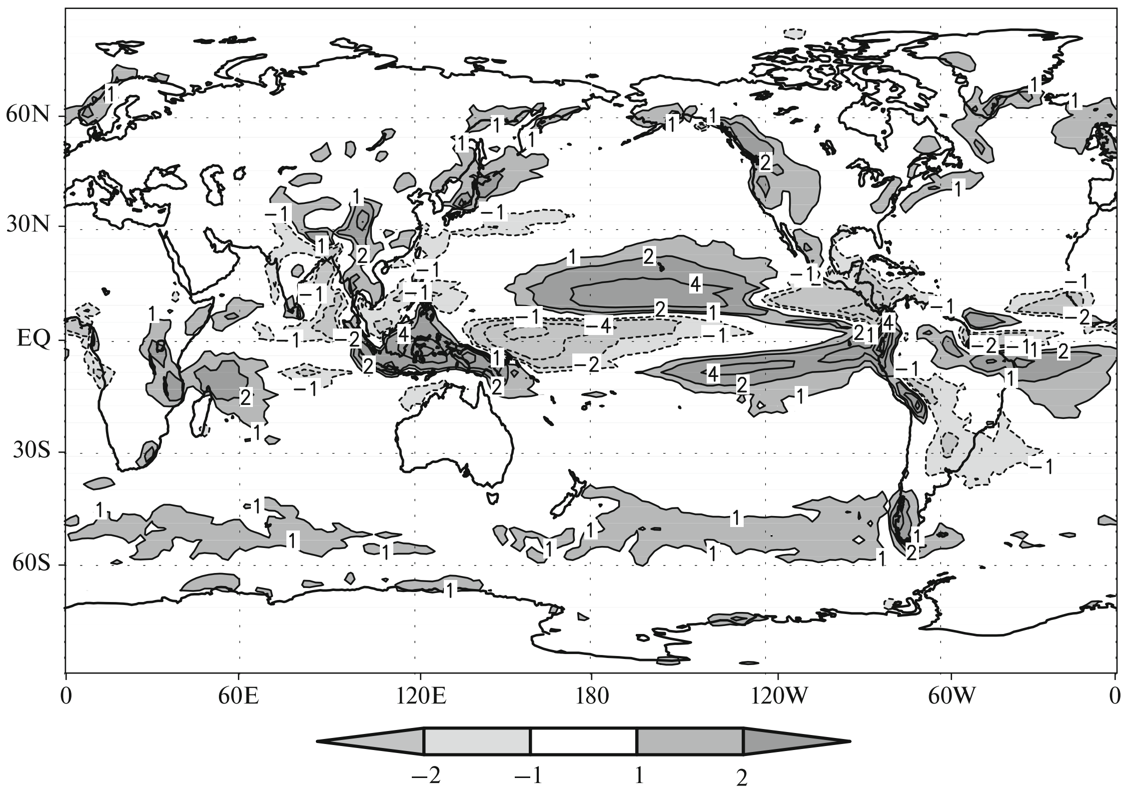

Fig. 2. Difference in the annual mean precipitation (mm/day) between the model values and the data [30].

of South America and the Atlantic coast of Africa) that is typical for most current climate models [6]. Overestimation of the NSAT in the Arctic Ocean (AO), as well as in some seas near the coast of the Antarctica, is a specific problem of the INMCM5.0 model and can be related to the fact that ice cohesion in these places is less than one by a few hundredths, even in the winter. The flow of sensible and latent heat from the part of the ocean surface that is not ice-covered significantly heats the lower layers of the Arctic and Antarctic atmosphere. The underestimation of the NSAT over the tropical and subtropical continents was reduced compared to the previous version. This happened due to changes in night temperature; daytime temperatures remained nearly unchanged. The reason for this is a change in stratification of the atmospheric boundary layer as a result of modification in parameterization of its involvement on the upper boundary, as well as modifications in clouds and condensation. The root-mean-square error in the average annual temperature was 1.84 K in the INMCM4 model, while in the INMCM5 model it had fallen to 1.59 K.

The spatial distribution of the difference between the model and observed precipitations (Fig. 2) is approximately the same as in the previous version of the model. In the tropics, the errors in simulated precipitations, which are related to the position of the convergence zone, lead to the overestimation of precipitations over the western part of the Indian Ocean and their underestimation over the eastern part, overestimation of precipitation in the Pacific Ocean off the equator and their underestimation near the equator, and underestimation in the Atlantic north of the equator and overestimation to the south the equator. As can be seen, for example, in [6] (Fig. 11.4b), such errors are typical for most modern models. At the same time, overestimation of precipitation in the temperate latitudes of both hemispheres is a specific feature of the INMCM5 model and its previous versions. The values of the errors in the INMCM5 remained approximately the same as in the INMCM4 model [3] (Fig. 2) or decreased slightly. This is especially noticeable in the west of the Indian Ocean and on the south branch of the convergence zone in the Pacific Ocean. The rms error in the annual mean rainfall is 0.89 mm/day in the INMCM5 model and was 1.03 mm/day in the INMCM4 model.

The error in zonal temperature and wind speed at different altitudes is shown in Fig. 3. If one compares it with a similar error in the previous versions of the model ([3], Fig. 4), it can be seen that errors in the troposphere remained approximately the same in value and location, or even slightly increased. The apparent increase of the negative error in the lower troposphere temperature near 30°–40° N is associated with the choice of the ERA reanalysis for observation instead of the NCEP. Different extrapolation procedures were used in these two reanalysis data for the pressure levels below the ground. In the lower stratosphere, the errors

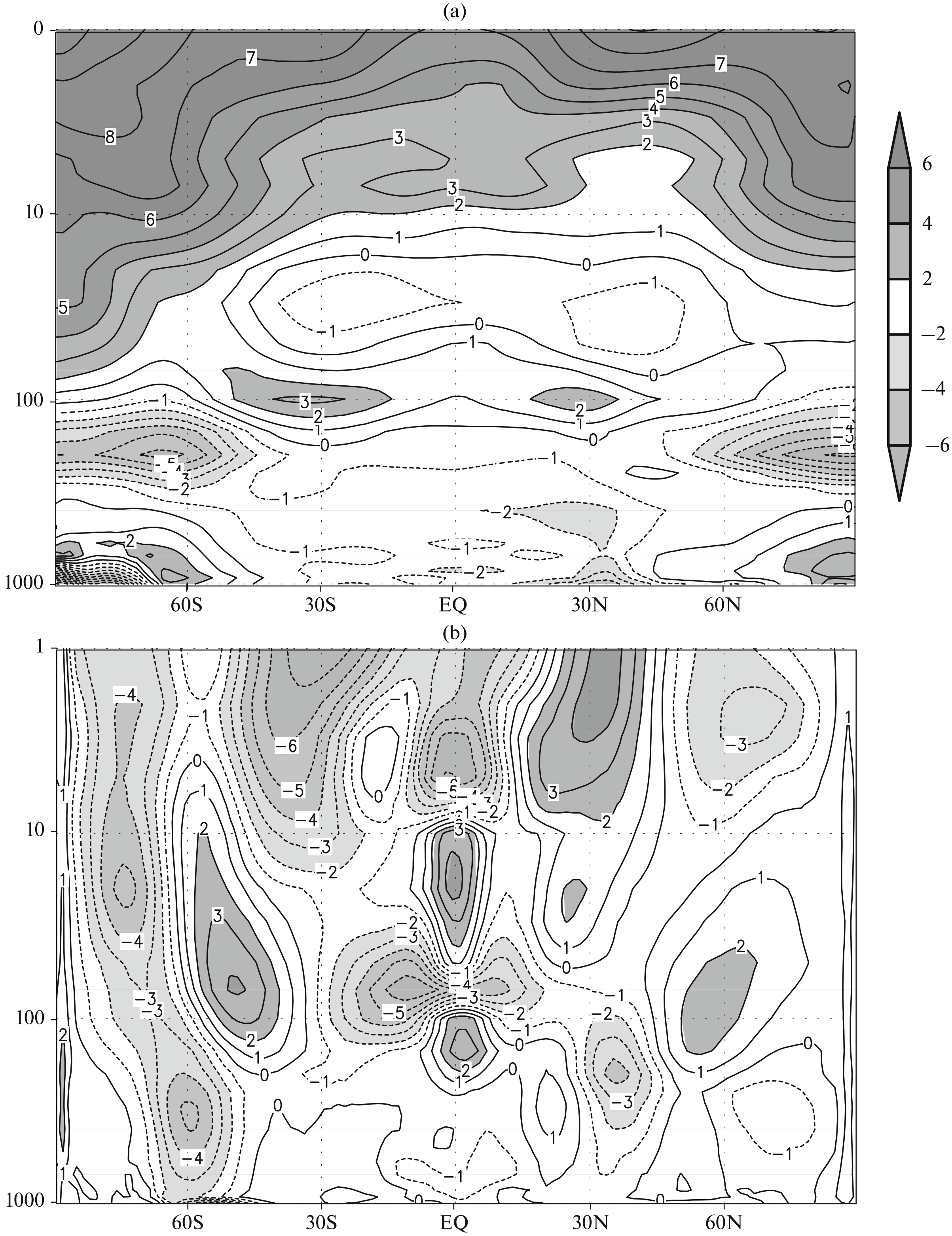

Fig. 3. Difference in (a) the annual mean temperature (K) and (b) speed of zonal wind (m/s) between the model (averaged along the latitudinal circle) and the ERA reanalysis data.

in the latest version of the model slightly decreased compared to the previous version. This is due to the fact that some parameterizations (primarily those of orographic gravity-wave drag and deep convection) were adjusted so as to reduce the errors in temperature and wind speed near the tropopause and in the lower

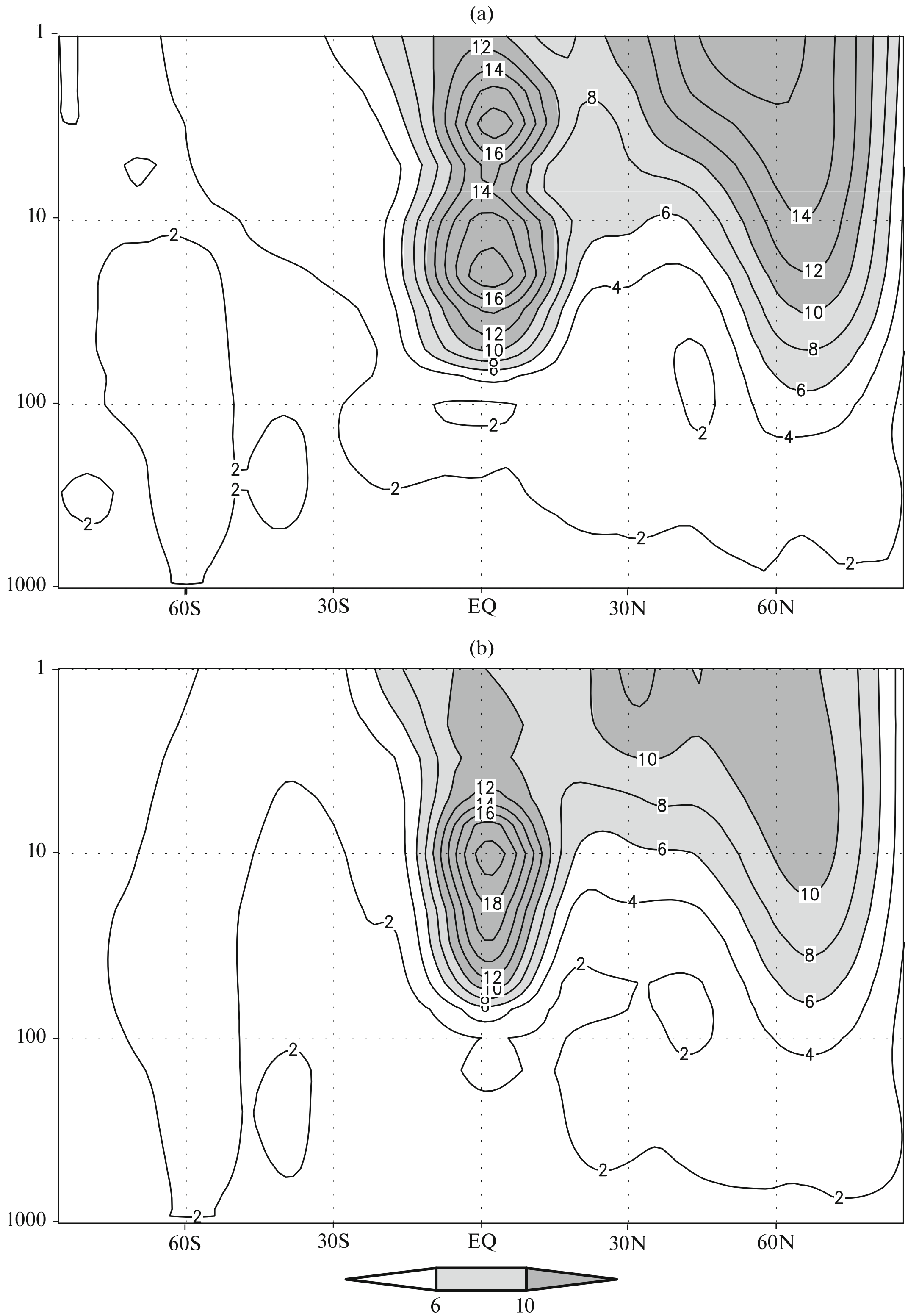

Fig. 4. Standard deviation of the monthly average speed of zonal wind (averaged along the latitudinal circle) (m/s) in December–February according to the (a) ERA reanalysis data and (b) results of the model.

stratosphere. For example, the reduction of errors in temperature near the tropical tropopause is related to the fact that the upper boundary of deep convection in its parameterization is located slightly above the level of neutral buoyancy, which accounts for air lifting by inertia. The increased error in the zonal wind speed in

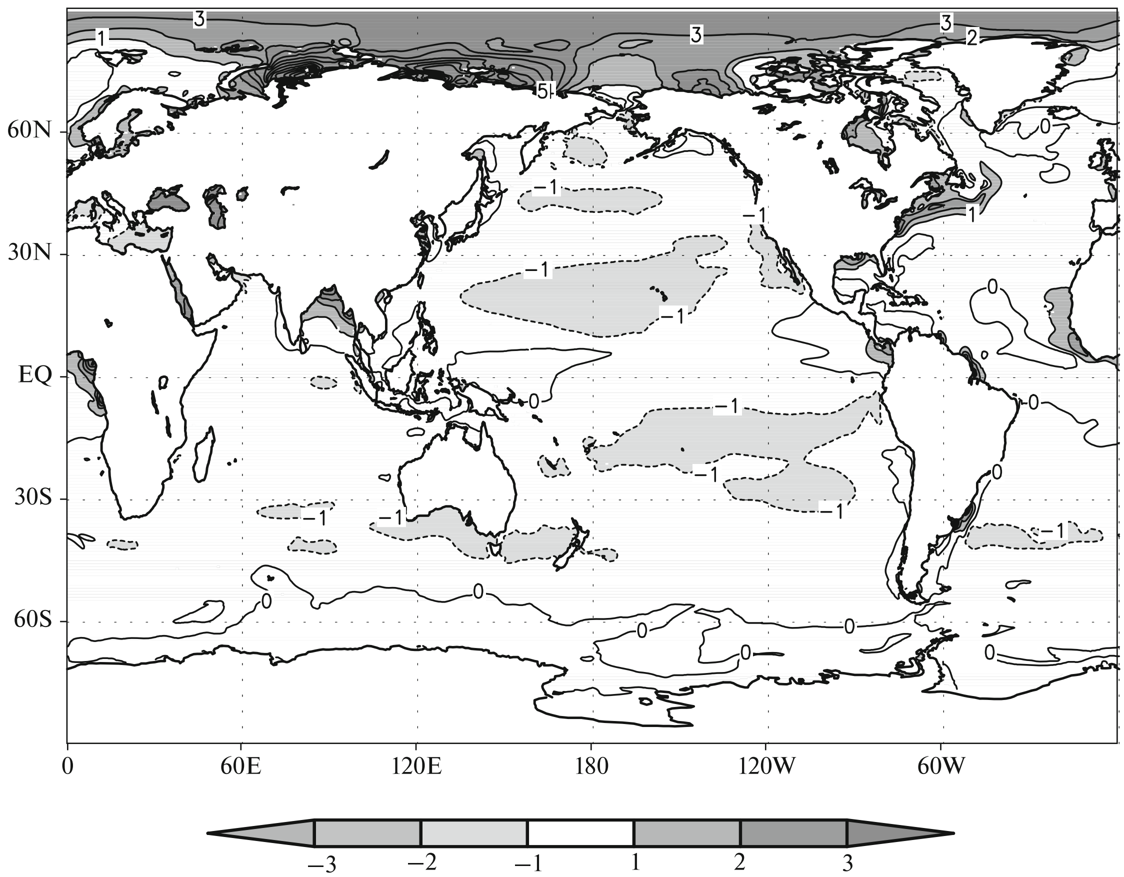

Fig. 5. Difference in surface salinity (PSU) between the model and observations [24].

the upper troposphere near 40° N is due, apparently, to insufficient tuning of the parameterization of gravity-wave drag. In the upper stratosphere, the temperature error reaches 5°–8°. However, larger values of temperature and wind-speed errors in the upper stratosphere compared to the levels located below is typical for climate models.

The root-mean-square deviations in zonal wind velocity in December–February for the model and ERA reanalysis are presented in Fig. 4. The maximum standard deviation in the equatorial stratosphere at the levels of 5–70 hPa, reaching 12–18 m/s, is caused by quasi-biennial oscillation. Its amplitude, period of 2–2.5 years, and downward spread of phase of the fluctuation are well reproduced in the model. Reproduction of this phenomenon requires the adjustment of parameterization of nonorographic gravity-wave drag, horizontal and vertical diffusion, and sufficiently detailed vertical resolution in the lower stratosphere (at least 500 m).

In the temperate latitudes of the winter hemisphere, the stratospheric variability of wind speed, according to the data of observations, reaches of 16 m/s, while according to the model it is 12 m/s. This type of variability is due to the interaction of Rossby waves propagating from the bottom with an average flow. The rms deviation of the wind speed is somewhat underestimated in the model. The amplitude of waves number 1 and 2 is also understated in the model by a factor of 1.1–1.5. Sudden stratospheric warming (SSW) is one of the most striking manifestations of this variability. The presence of easterly wind instead of the usual westerly wind at 60° N on the surface of 10 hPa in the winter months is generally considered a criterion for the SSW. According to the observations, there were 18 SSW events in 30 years. In the model, there were 33 SSWs in 80 years, thus, the frequency of the SSW occurrence in the model is 1.4–1.5 times lower than in nature. According to the comparison of dynamics of the stratosphere in climate models [33] and in models with a high enough upper boundary (above 40 km), the number of the SSWs in 30 years is generally 10 to 25, and on average it is close to the observed value of 18. A more detailed description of reproduction of stratospheric dynamics in the atmospheric block of the INM RAS climate model can be found in [34].

3.2. Ocean

The error in salinity on the ocean surface is shown in Fig. 5. The negative error in salinity of most of the ocean, which is typical for the majority of climate models, has decreased considerably in the last version of the

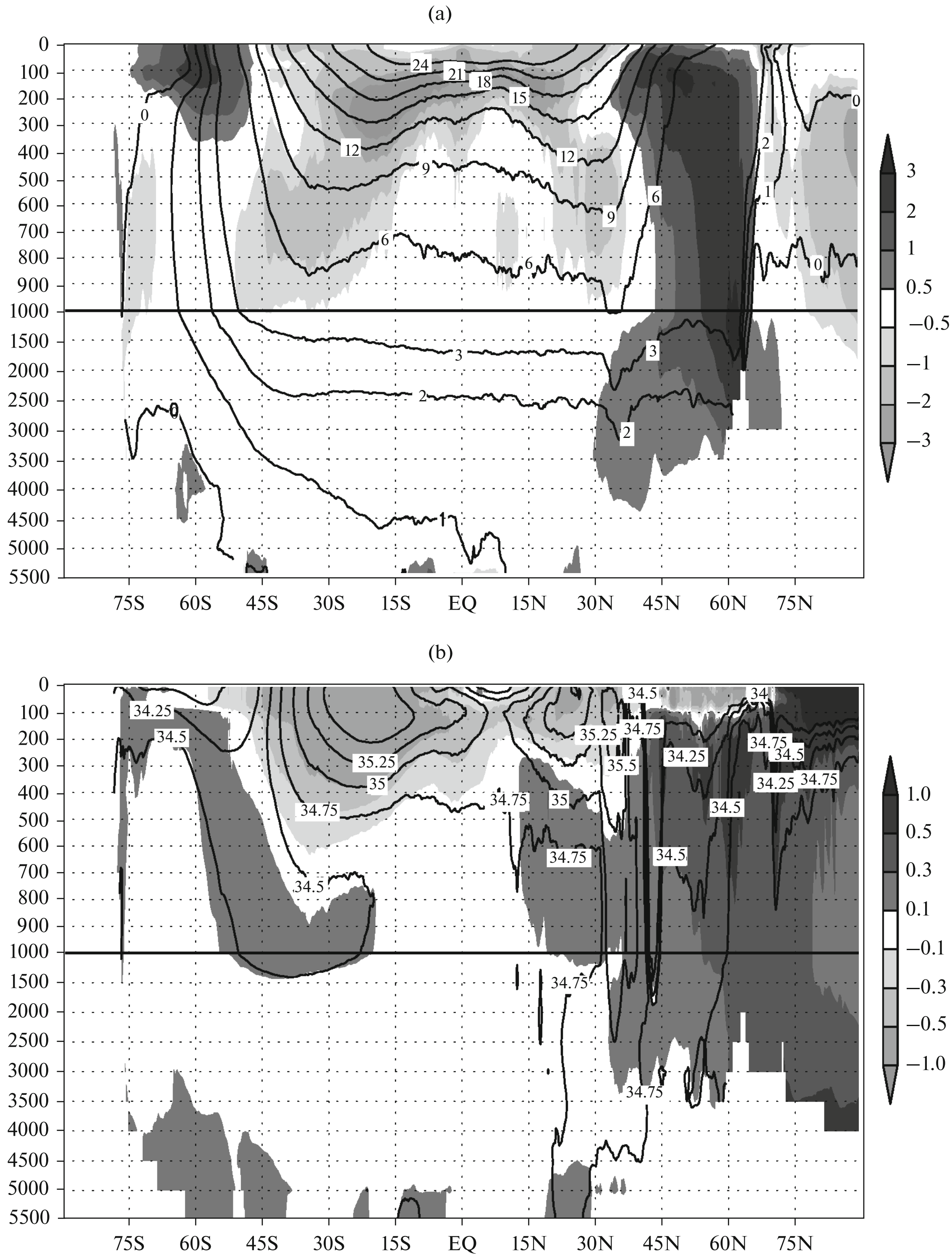

Fig. 6. (a) Zonal mean deviation of the potential ocean temperature in the model (°C, gradations of gray with the scale on the right from the panel) from the annual mean climatic distribution according to the data [35] (isolines, °C). (b) The same for salinity (deviations are shown in gradations of gray and the data are shown by isolines).

model compared to the previous one ([3], Fig. 1b). At the same time, the positive error in salinity of the AO has increased. It seems that this error is caused by the same problem of sea-ice simulation, which is responsible for the error in the NSAT in the AO. Due to the underestimated value of sea-ice cohesion, the model shows the excessive formation of new ice with respected salt release, which leads to an error in salin-

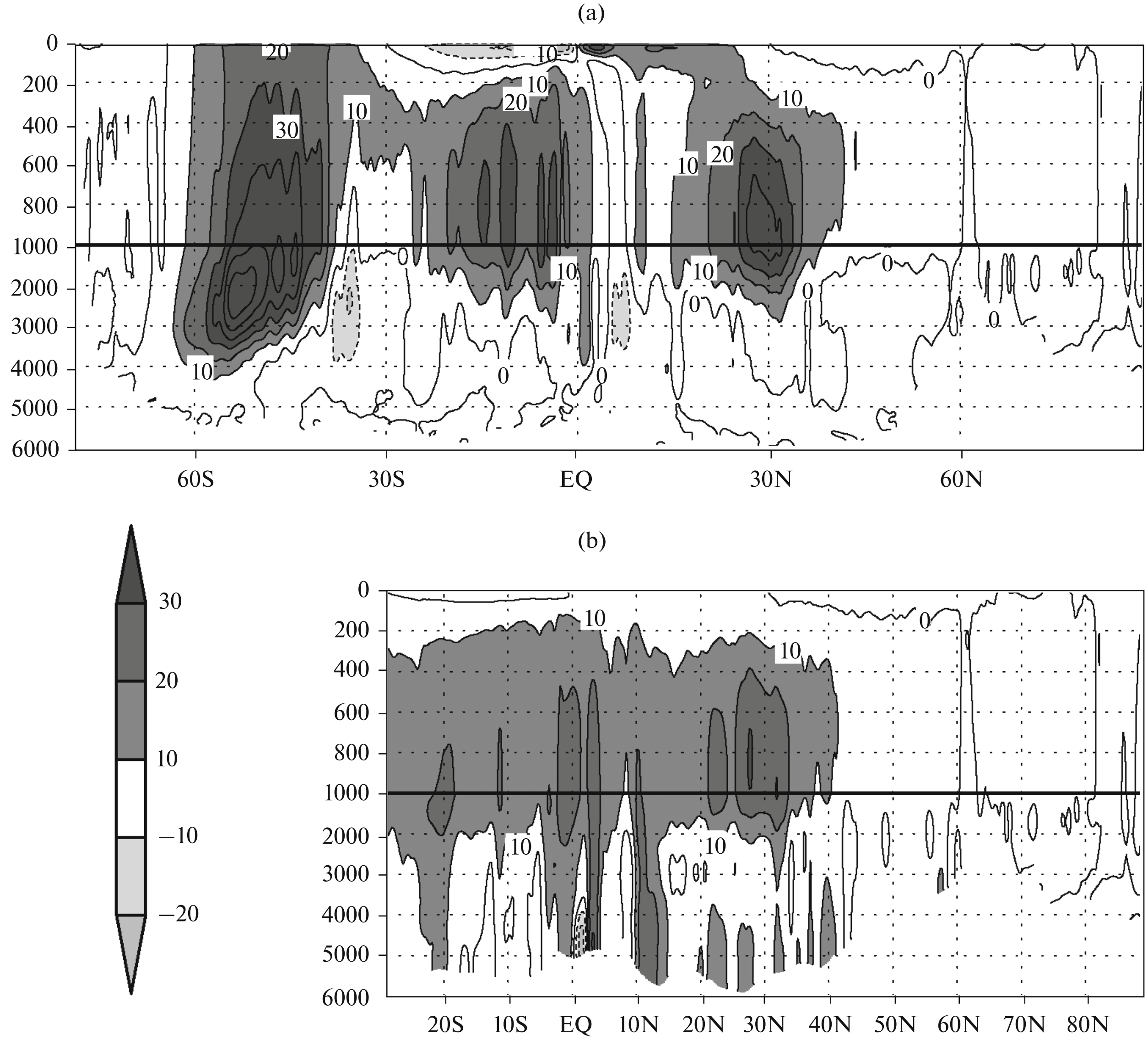

Fig. 7. Meridional stream function (Sv) according to the model data: (a) in the World Ocean and (b) in the Atlantic.

ity. The salinity rms error in the latest version of the model is 0.78 PSU and, in the previous version, 1.20 PSU. The improvement is due to an increase in resolution in the ocean.

Figure 6 shows zonal mean errors in simulation of potential temperature and salinity in the ocean against zonal mean climatic values from [35]. In the tropical ocean, below a depth of 1 km, the error in temperature does not exceed 0.5°, while the previous version of the model underestimated the temperature at the bottom and overestimate it at depths of 500–1500 m by 1°–3°. The improvement is due to taking into account the dependence of the background factor of vertical diffusion on depth.

At the surface, especially in the tropics and subtropics, the water in the model is colder and fresher than in the observational data. The main error in temperature is confined to the middle latitudes of the Northern Hemisphere, in the belt of 45°–60° N. Apparently, this error is generated in the surface layers and extends from the surface to the bottom due to processes of deep convection. In general, values of the errors in temperature and salinity agree with the model average errors presented in [6] (Fig. 9.13). However, their spatial distribution in the INMCM5.0 is somewhat different. For example, deviations of the model mean temperatures at depths of 200–1000 m are positive and extend from the Southern Ocean to the North Pole, while in the INMCM5.0 they are negative in the tropics and subtropics (Fig. 8a). The error pattern of salinity in the INMCM5.0 is more consistent with that in multi-model, except for the AO near-surface layers, where it is positive due to the abovementioned reasons; the model mean error is negative.

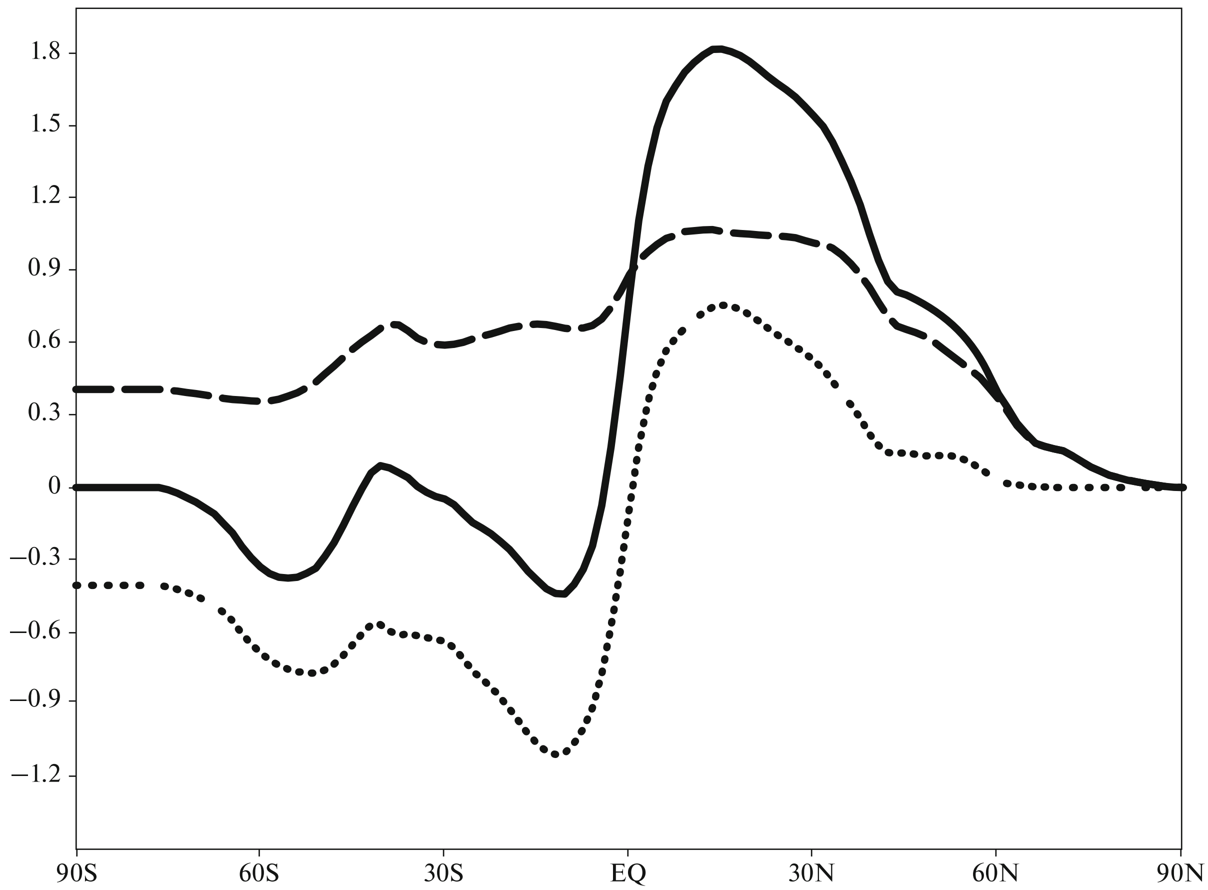

Fig. 8. Heat flux to the North (10^{15} W) in the World Ocean (solid curve), Atlantic Ocean (dashed curve), and Pacific and Indian oceans (dotted curve).

The meridional circulation stream function for the World Ocean and the Atlantic sector is shown in Fig. 7. Circulation cells are clearly visible at the surface; they are caused by wind stress on the surface. The cell extends to a depth of 3000 m in the southern temperate latitudes. In the rest of the ocean, the mass transfer occurs from south to north in a layer of 200–1000 m, and from north to south, in a deeper layer, from 1500 to 3000 m. Nearly all this transfer is caused by circulation in the Atlantic. The mass flow here is more than 20 Sv, which is close to estimations from observations [36] (15–20 Sv). Changes in the meridional stream function, as compared to the previous version of the INMCM4.0 model, manifest themselves in strengthening of the North Atlantic cell and distortion of the picture in the Southern Ocean when the maximum of zonal circulation has shifted from the surface to a depth of 2500 m; this indicates the deterioration of the meridional circulation in the Southern Ocean.

Meridional heat transport in the ocean (Fig. 8) changed very slightly compared to the data of the previous version of the model ([3], Fig. 10). Heat transfer to the north in the Atlantic Ocean grew slightly, getting closer to the estimates from observations [25] than it was. This change is due to the mentioned intensification of the meridional stream function and is, apparently, also related to an increase in the resolution of the ocean model.

The analysis of reproduction of this version of the climate model, averaged over the sea-level time and its natural variability, is given in [37]. According to this analysis, the rms error in reproduction of the annual mean sea level has decreased from 0.26 m in the previous version of the model to 0.20 m in the latest version. As follows from this work, the rms error in sea level is getting smaller with a further increase of resolution in the ocean.

Figure 9 shows the standard deviation of the monthly average surface temperatures in the tropical Pacific Ocean according to the NCEP reanalysis and the model. The maximum value of standard deviation in the equatorial Pacific from observations is about 1.2 K, and according to the model it is 0.8–0.9 K, i.e., slightly smaller than observations. Compared with the previous version, the geographic distribution of El Niño is in better agreement with observations. It ceased propagating to the west of the Pacific Ocean, and the standard deviation grew near the coast of South America getting closer to the observed value. The reason for this improvement is an increase in the

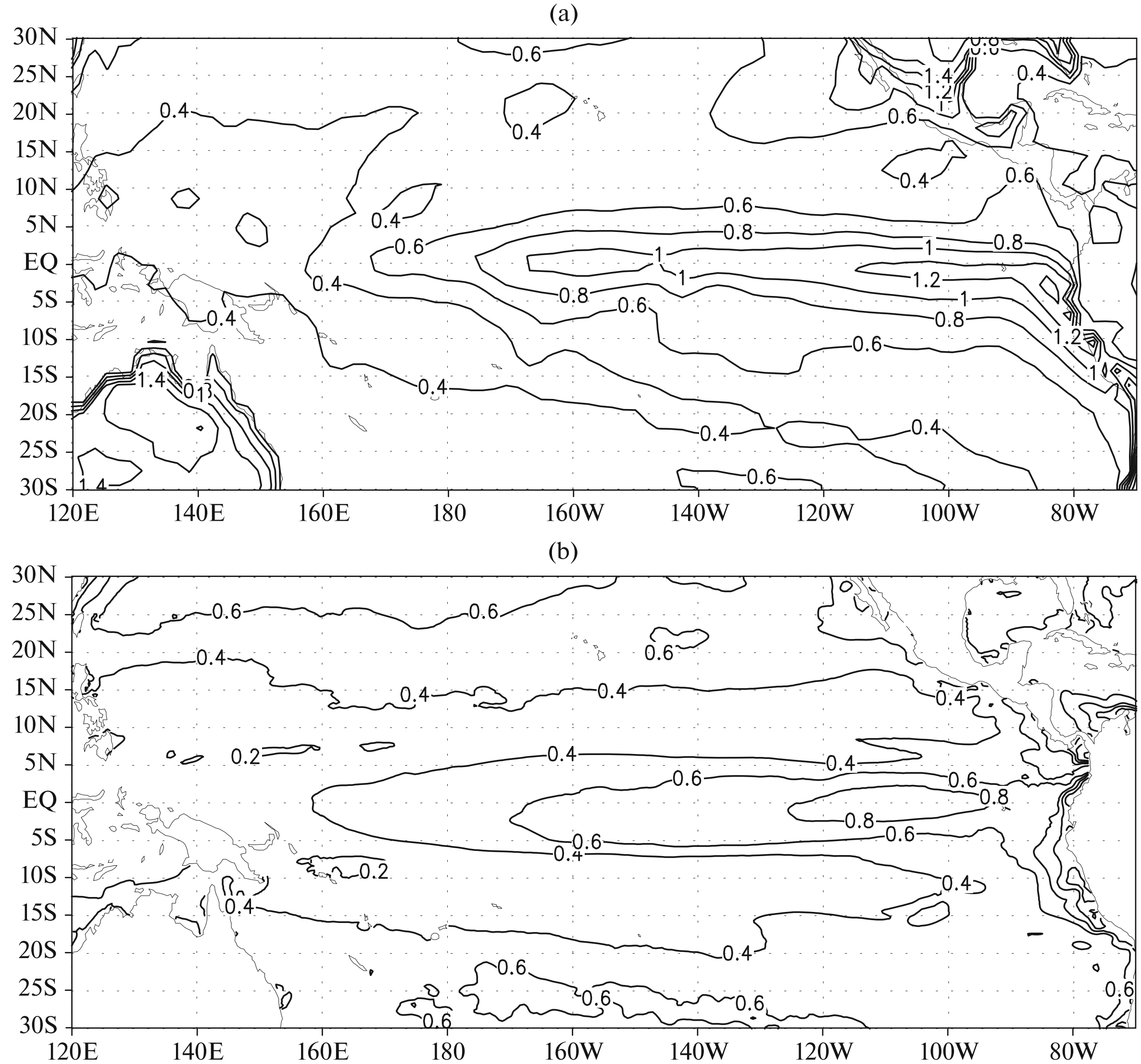

Fig. 9. Standard deviation of the monthly average temperature (K) in the tropical area of the Pacific Ocean according to the (a) NCEP reanalysis and (b) model results.

spatial resolution of the ocean model. The underestimation in the El Niño amplitude by the model needs further investigation.

According to the observations, El Niño occurs every 2–7 years. The model reproduces this feature; however, in the model, El Niño occurs on average more regularly than in the observations. The observed time series has a well-pronounced positive asymmetry: the values of positive extrema are markedly larger than the values of negative ones, while in the model data asymmetry is close to zero. The reasons for this discrepancy require further investigation.

4. CONCLUSIONS

The INMCM5 climate model is created, and it differs from the previous version by a higher upper boundary of the atmosphere and more detailed vertical resolution in the stratosphere. Horizontal resolution of the ocean model is increased. Furthermore, the scheme for simulation of clouds and condensation is modified in the atmospheric model, and an aerosol block is added. A numerical experiment is carried out with the model to reproduce the current climate over 80 years. It has been shown that some systematic errors have decreased due to increase in the spatial resolution and implementation of new parameterizations. The reproduction of some phenomena, first and foremost, the quasi-biennial oscillation of the wind speed in the equatorial stratosphere and sudden stratospheric warmings, has become possible due to the improvement of the vertical resolution in the atmospheric block. At the same time, some errors, including those in the global mean values, remained at the same level or even slightly increased. For example, a distorted picture of the meridional stream function in the Southern Ocean requires a separate study. Overall, the new version of the climate model is ready to take part in numerical experiments for the simulation of the climate and its changes within the CMIP6 program.

ACKNOWLEDGMENTS

Development of model INMCM5 was performed in INM RAS and supported by Russian Scientific Foundation (grant 14-17-00126). Numerical experiments are performed at supercomputer of Joint Supercomputer Center of RAS and supported by Government of Russian Federation (agreement 14.Z50.31.0033 with Institute of Applied Physics RAS).

REFERENCES

1. M. I. Budyko, *Climate of the Past and Future* (Gidrometeoizdat, Leningrad, 1980) [In Russian].
2. I. I. Mokhov and A. V. Eliseev, "Modeling of global climate variations in the 20th–23rd centuries with new RCP scenarios of anthropogenic forcing," Dokl. Earth Sci. **443** (2), 532–536 (2012).
3. E. M. Volodin, N. A. Diansky, and A. V. Gusev, "Simulating present-day climate with the INMCM4.0 coupled model of the atmospheric and oceanic general circulations," Izv., Atmos. Ocean. Phys. **46** (4), 414–431 (2010).
4. K. E. Taylor, R. J. Stouffer, and G. A. Meehl, "An overview of CMIP5 and the experiment design," Bull. Am. Meteorol. Soc. **93**, 485–498 (2012).
5. E. M. Volodin, N. A. Diansky, A. V. Gusev, "Simulation and prediction of climate changes in the 19th to 21st centuries with the Institute of Numerical Mathematics, Russian Academy of Sciences, Model of the Earth's climate system," Izv., Atmos. Ocean. Phys. **49** (4), 347–366 (2013).
6. G. Flato, J. Marotzke, B. Abiadun, et al., "Evaluation of climate models," in *Climate Change 2013: The Physical Science Basis. Contribution of Working Group I to the Fifth Assessment Report of the Intergovernmental Panel on Climate Change* (Cambridge Univ. Press, Cambridge, 2013), pp. 741–866.
7. V. A. Alekseev, E. M. Volodin, V. Ya. Galin, V. P. Dymnikov, and V. N. Lykosov, *Modern Climate Simulation Using the INM RAS Atmospheric Model*, Preprint No. 2086-B98 (Institute of Numerical Mathematics, Russian Academy of Sciences, Moscow, 1998) [In Russian].
8. V. Ya. Galin, E. M. Volodin, and S. P. Smyshlyaev, "The INM RAS atmospheric general circulation model with ozone dynamics," Meteorol. Gidrol., No. 5, 13–23 (2003).
9. V. Ya. Galin, "Parametrization of radiative processes in the DNM atmospheric model," Izv., Atmos. Ocean. Phys. **34** (3), 339–347 (1998).
10. A. K. Betts, "A new convective adjustment scheme. Part 1. Observational and theoretical basis," Q. J. R. Meteorol. Soc. **112**, 677–691 (1986).
11. T. N. Palmer, G. J. Shutts, and R. Swinbank, "Alleviation of a systematic westerly bias in general circulation and numerical weather prediction models through an orographic gravity wave drag parameterization," Q. J. R. Meteorol. Soc. **112**, 1001–1031 (1986).
12. C. O. Hines, "Doppler spread parameterization of gravity wave momentum deposition in the middle atmosphere. 2. Broad and quasimonochromatic spectra, and implementation," J. Atmos. Sol.–Terr. Phys. **59**, 387–400 (1997).
13. M. Tiedtke, "Representation of clouds in large-scale models," Mon. Weather Rev. **121**, 3040–3061 (1993).
14. E. M. Volodin and S. V. Kostrykin, "The aerosol module in the INM RAS climate model," Russ. Meteorol. Hydrol. **41** (8), 519–528 (2016).
15. N. A. Diansky, *Modeling of the Ocean Circulation and Study of Its Response to Short-Period and Long-Period Atmospheric Impacts* (Fizmatlit, Moscow, 2013) [in Russian].
16. V. B. Zalesny, G. I. Marchuk, V. I. Agoshkov, A. V. Bagno, A. V. Gusev, N. A. Diansky, S. N. Moshonkin, R. Tamsalu, and E. M. Volodin, "Numerical simulation of large-scale ocean circulation based on the multicomponent splitting method," Russ. J. Numer. Anal. Math. Modell. **25** (6), 581–609 (2010).
17. K. M. Terekhov, E. M. Volodin, and A. V. Gusev, "Methods and efficiency estimation of parallel implementation of the σ-model of general ocean circulation," Russ. J. Numer. Anal. Math. Modell. **26** (2), 189–208 (2011).
18. N. G. Yakovlev, "Reproduction of the large-scale state of water and sea ice in the Arctic Ocean in 1948–2002: Part I. Numerical model," Izv., Atmos. Ocean. Phys. **45** (3), 357–371 (2009).
19. E. V. Mortikov, "Increasing the scalability of the program complex of the Earth system model of high spatial resolution," in *Parallel Computing Technologies (PaVT'2015): Proceedings of International Scientific Conference* (YuUrGu, Chelyabinsk, 2015), pp. 431–435.
20. A. A. Mirin and P. H. Worley, "Improving the performance scalability of the community atmosphere model," Int. J. High Perform. Comput. Appl. **26** (1), 17–30 (2012).
21. S. M. Uppala, P. W. Kallberg, A. J. Simmons, et al., "The ERA-40 reanalysis," Q. J. R. Meteorol. Soc. **131** (612), 2961–3012 (2005).
22. E. Kalnay, M. Kanamitsu, R. Kistler, et al., "The NCEP/NCAR 40 year reanalysis project," Bull. Am. Meteorol. Soc. **77** (3), 437–471 (1996).
23. P. Xie and P. A. Arkin, "Global precipitation: A 17-year monthly analysis based on gauge observations, satellite estimates, and numerical model outputs," Bull. Am. Meteorol. Soc. **78**, 2539–2558 (1997).
24. M. Steele, R. Morley, and W. Ermold, "PHC: A global ocean hydrography with a high quality Arctic Ocean," J. Clim. **14**, 2079–2087 (2001).
25. K. E. Trenbeth and J. M. Caron, "Estimates of meridional atmosphere and ocean heat transports," J. Clim. **14** (16), 3433–3443 (2001).
26. Hartmann D.L., Klein A., Rusticucci M. et al. Observations: Atmosphere and Surface. In: Climate Change

2013: The Physical Science Basis. Contribution of Working Group I to the Fifth Assessment Report of the Intergovernmental Panel on Climate Change. Cambridge: Cambridge University Press: 2013. P. 159–254.

27. A. V. Chernokul'skii and I. I. Mokhov, "Comparative analysis of global and zonal cloudiness characteristics according to different satellite and ground-based observation data," Issled. Zemli Kosmosa, No. 3, 12–29 (2010).
28. K. E. Trenberth, L. Smith, T. Qian, A. Dai, J. Fasullo, "Estimates of the global water budget and its annual cycle using observational and model data," J. Hydrometeorol. **8** (4), 758–769 (2007).
29. D. A. Robinson, K. F. Dewey, and R. R. Heim, "Global snow cover monitoring: An update," Bull. Am. Meteorol. Soc. **74** (9), 1689–1696 (1993).
30. T. Zhang, R. G. Barry, K. Knowles, et al., "Statistics and characteristics of permafrost and ground-ice distribution in the Northern Hemisphere," Polar Geogr. **23** (2), 132–154 (1999).
31. T. Zhang, R. G. Barry, K. Knowles, et al., "Distribution of seasonally and perennially frozen ground in the Northern Hemisphere," in *Permafrost: Proceedings of the Eighth International Conference on Permafrost*, Ed. by M. Phillips, S. M. Springman, L. U. Arenson (Taylor and Francis, London, 2003), pp. 1289–1294.
32. N. A. Rayner, D. E. Parker, E. B. Horton, C. K. Folland, L. V. Alexander, D. P. Rowell, E. C. Kent, and A. Kaplan, "Global analyses of sea surface temperature, sea ice, and night marine air temperature since the late nineteenth century," J. Geophys. Res. **108** (D14), 4407 (2003). doi 10.1029/2002JD002670
33. N. Butchart, N. Butchart, A. J. Charlton-Perez, I. Cionni, et al., "Multimodel climate and variability of the stratosphere," J. Geophys. Res. **116**, D05102 (2011). doi 10.1029/2010JD014995
34. P. N. Vargin and E. M. Volodin, "Analysis of the reproduction of dynamic processes in the stratosphere using the climate model of the Institute of Numerical Mathematics, Russian Academy of Sciences," Izv., Atmos. Ocean. Phys. **52** (1), 1–15 (2016).
35. T. P. Boyer, J. I. Antonov, O. K. Baranova, H. E. Garcia, D. R. Johnson, R. A. Locarnini, A. V. Mishonov, T. D. O'Brien, D. Seidov, I. V. Smolyar, and M. M. Zweng, *World Ocean Database 2009, NOAA Atlas NESDIS 66*, Ed. by S. Levitus (NOAA, Washington, D.C., 2009).
36. G. A. Meehl, T. F. Stocker, W. D. Collins, et al., "Global climate projections," in *Climate Change 2007. The Physical Science Basis* (Cambridge University Press, Cambridge, 2007), pp. 748–845.
37. N. G. Yakovlev, E. M. Volodin, and A. S. Gritsun, "Simulation of the spatiotemporal variability of the World Ocean sea surface height by the INM climate models," Izv., Atmos. Ocean. Phys. **52** (4), 376–385 (2016).

Translated by I. Ptashnik